scheme shows directly that the only graphs that contribute to the renormalization of γ_0, beyond those arising from the wave-function renormalization Z', must include a factor of the bulk interaction g_0; this implies that $Z_\gamma = 1$ for $g = 0$, and shows that for the models of (*9, 10*) the one-loop exponent $\eta' = \epsilon$ is exact.

The above methods can be extended to determine the behavior of other observables in the regimes of Fig. 3. We mention a few as follows.

1) Entropy: In the paramagnetic phase ($\lambda < \lambda_c$), there is clearly a residual entropy of $\ln(2S + 1)$ as $T \to 0$. At $\lambda = \lambda_c$, the ϵ expansion shows that this is modified to $\ln(2S + 1) - S(S + 1)(33\epsilon/160)^{1/2} + O(\epsilon^{3/2})$, whereas in the Néel state ($\lambda > \lambda_c$, the Néel order pinned by some small spin anisotropy) the impurity entropy vanishes as T^d at low T.

2) Knight shift: We restrict the discussion here to the intermediate quantum-critical region of Fig. 3, $T > |\lambda - \lambda_c|^\nu$. The shift in the nuclear magnetic resonance frequency is proportional to the local response in the presence of a uniform external field, $\chi(x)$. In the vicinity of the impurity (for example, at site $i = Y$), $\chi(x) \sim T^{-1+\eta'/2}$. Well away from the impurity ($|x| \to \infty$), apart from the bulk response of the antiferromagnet, there are staggered and uniform contributions that decay exponentially with $|x|$ on a scale $\sim \hbar c/(\sqrt{\epsilon} k_B T)$.

3) Magnon damping: In the quantum paramagnet ($\lambda < \lambda_c$), and at $T = 0$, the pure antiferromagnet has a pole in the dynamic spin structure factor $\sim 1/(\Delta - \hbar\omega)$ at the antiferromagnetic ordering wavevector from the triplet magnon excitations. In the presence of a dilute concentration of impurities, n_i, this pole will be broadened on an energy scale Γ; scaling arguments and the structure of the fixed point found here imply the exact form (*23*) $\Gamma \sim n_i(\hbar c)^d \Delta^{1-d}$. We argue that this damping mechanism is the main ingredient in the broadening of the resonance peak observed recently in Zn-doped $YBa_2Cu_3O_7$ (*24*). Using the values $\hbar c = 0.2a$ eV (a is the lattice spacing), $\Delta = 40$ meV, and $n_i = 0.005/a^2$, we obtain the estimate $\Gamma = 5$ meV, which is in excellent accord with the observed line width of 4.25 meV (*24*). We have also studied the line shape of the magnon peak (*17*) and find that it is asymmetric at very low T, with a tail at high frequencies; it would be interesting to test this in future experiments.

We have described the highly nontrivial, collective, quantum spin dynamics of a single impurity in a strongly correlated, low-dimensional electronic system. The problem maps onto a new boundary quantum field theory (Eqs. 9 and 10) and is therefore also of intrinsic theoretical interest. Unlike previously studied quantum impurity problems, there is a complicated interference between bulk and boundary interactions, and its proper description is the key to the physical results we have obtained. Our theoretical results for the magnon damping in the spin-gap phase are in good agreement with existing experiments (*24*). Studies of materials exhibiting other aspects of the regimes of Fig. 3 appear possible, and we hope they will be undertaken; spin-gap compounds can be driven across the transition by, say, application of hydrostatic pressure or by doping with other impurities that have the same spin as the host ion they replace and do not change the sign of the exchange constants (*25*). Quantum Monte Carlo simulations should also allow more accurate determination of the universal constants C_1 and C_3.

References and Notes

1. E. Dagotto and T. M. Rice, *Science* **271**, 618 (1996).
2. A. M. Finkelstein, V. E. Kataev, E. F. Kukovitskii, G. B. Teitel'baum, *Physica C* **168**, 370 (1990).
3. H. Alloul, P. Mendels, H. Casalta, J. F. Marucco, J. Arabski, *Phys. Rev. Lett.* **67**, 3140 (1991); A. V. Mahajan, H. Alloul, G. Collin, J. F. Marucco, *Phys. Rev. Lett.* **72**, 3100 (1994); D. L. Sisson *et al*., preprint available at http://xxx.lanl.gov/abs/cond-mat/9904131; J. Bobroff *et al*., preprint available at http://xxx.lanl.gov/abs/cond-mat/9906152.
4. M. Hase, I. Terasaki, Y. Sasago, K. Uchinokura, H. Obara, *Phys. Rev. Lett.* **71**, 4059 (1993); S. B. Oseroff *et al*., *Phys. Rev. Lett.* **74**, 1450 (1995); K. M. Kojima *et al*., *Phys. Rev. Lett.* **79**, 503 (1997); T. Masuda, A. Fujioka, Y. Uchiyama, I. Tsukada, K. Uchinokura, *Phys. Rev. Lett.* **80**, 4566 (1998); Y. Uchiyama *et al*., *Phys. Rev. Lett.* **83**, 632 (1999).
5. N. Read and S. Sachdev, *Phys. Rev. Lett.* **62**, 1694 (1989); *Phys. Rev. Lett.* **66**, 1773 (1991).
6. N. Katoh and M. Imada, *J. Phys. Soc. Jpn.* **63**, 4529 (1994); M. Imada and Y. Iino, *J. Phys. Soc. Jpn.* **66**, 568 (1997); J. Tworzydlo, O. Y. Osman, C. N. A. van Duin, J. Zaanen, *Phys. Rev. B* **59**, 115 (1999); S. Sachdev and M. Vojta, preprint available at http://xxx.lanl.gov/abs/cond-mat/9908008.
7. S. Sachdev, *Quantum Phase Transitions* (Cambridge Univ. Press, Cambridge, 1999); *Phys. World* **12** (April), 33 (1999).
8. A. W. Sandvik, E. Dagotto, D. J. Scalapino, *Phys. Rev. B* **56**, 11701 (1997).
9. S. Sachdev and J. Ye, *Phys. Rev. Lett.* **70**, 3339 (1993); A. Georges, O. Parcollet, S. Sachdev, preprint available at http://xxx.lanl.gov/abs/cond-mat/9909239.
10. A. M. Sengupta, preprint available at http://xxx.lanl.gov/abs/cond-mat/9707316.
11. J. L. Smith and Q. Si, *Europhys. Lett.* **45**, 228 (1999).
12. P. Nozières and A. Blandin, *J. Phys. (Paris)* **41**, 193 (1980).
13. I. Affleck and A. W. W. Ludwig, *Nucl. Phys. B* **360**, 641 (1991); O. Parcollet, A. Georges, G. Kotliar, A. Sengupta, *Phys. Rev. B* **58**, 3794 (1998).
14. P. W. Anderson, *Phys. Rev.* **124**, 41 (1961).
15. For a clear and complete discussion of this point, see V. Barzykin and I. Affleck, *Phys. Rev. B* **57**, 432 (1998).
16. A. V. Chubukov and S. Sachdev, *Phys. Rev. Lett.* **71**, 169 (1993).
17. M. Vojta, C. Buragohain, S. Sachdev, preprint available at http://xxx.lanl.gov/abs/cond-mat/9912020.
18. J. L. Cardy, *Scaling and Renormalization in Statistical Physics* (Cambridge Univ. Press, Cambridge, 1996), chap. 7.
19. H. W. Diehl, in *Phase Transitions and Critical Phenomena*, C. Domb and J. Lebowitz, Eds. (Academic Press, London, 1986), vol. 20, pp. 75–264.
20. H. W. Diehl and S. Dietrich, *Z. Phys. B* **42**, 65 (1981).
21. E. Brézin, J. C. Le Guillou, J. Zinn-Justin, in *Phase Transitions and Critical Phenomena*, C. Domb and M. S. Green, Eds. (Academic Press, London, 1976), vol. 6, pp. 127–244.
22. S. Sachdev, *Phys. Rev. B* **55**, 142 (1997).
23. More precisely, the theory in Eqs. 9 and 10 predicts that $\Gamma = C_4 n_i (\hbar c)^d \Delta^{1-d}$ where C_4 is a universal number, of order unity in $d = 2$. This result is independent of the coupling γ_0 between the bulk and the impurity.
24. H. F. Fong *et al*., *Phys. Rev. Lett.* **82**, 1939 (1999). As suggested by these authors, we are treating the superconductor as a spin-gap insulator; this is a good approximation because the resonance excitation does not couple efficiently to the superconducting quasiparticles.
25. L. P. Regnault, J. P. Renard, G. Dhalenne, A. Revcolevschi, *Europhys. Lett.* **32**, 579 (1995).

26. We thank I. Affleck, H. Alloul, H. Fukuyama, A. Georges, M. Imada, A. Kapitulnik, B. Keimer, A. Sengupta, and O. Starykh for useful discussions. Supported by NSF grant DMR 96-23181 and by the Deutsche Forschungsgemeinschaft (VO 794/1-1).

23 September 1999; accepted 10 November 1999

Ion Penetration of the Water-Oil Interface

Kai Wu, Martin J. Iedema, James P. Cowin*

Ions typically pass with difficulty from water into organic phases because of water's superior solvation power. This inhibits such processes as ion transport in batteries or in lipid bilayers of cells. Ion penetration across such an interface was studied with unusual structural control. Hydronium ions were soft-landed at 1 electron volt on cold films of 3-methylpentane ("oil") on a metal substrate. The field produced by these ions drove them through the films when warmed. Coadsorption of water (0.14 to 35 bilayers) inhibited the ion penetration by creating a solvation energy trap. A Born solvation model successfully predicted the trapping energies (0 to 38 kilojoules per mole).

Transport of ions across the interface of two immiscible phases is fundamentally important in biological membranes, electrochemistry, phase transfer catalysis, fuel cells, extraction of nuclear waste, and groundwater contamination (*1–6*). Typically, hydration and solvation strongly affect both the energetics and kinetics of the ion transport. The Born equation (*7*) led to a qualitative understanding of the ion-transfer energetics derived from the difference in the dielectric constants of the two phases. Attempts to improve this understanding (*8, 9*) have been experimentally complicated by constraints of charge neu-

trality (which requires simultaneous motion of counterions), difficulties of probing the buried interface, and the low solubility of ions in low-dielectric liquids. Theoretical efforts have been frustrated by ambiguous definition of the interface thickness and inadequate knowledge of the interfacial structure.

Here we report a direct experimental observation of the effect of hydration on the motion of hydronium ions (D_3O^+) across a water-oil interface and in the oil. We used a modified Born-type solvation model, combined with simple ion mobility and kinetics models, to simulate the experimental data. The model yielded excellent agreement with our experimental results.

The experimental concept is shown schematically in Fig. 1. Hydronium ions are placed on top of a thin film of 3-methylpentane (3MP), where they generate a collective, planar electric field. As the assembly is warmed above the glass transition temperature of 3MP, this field will pull the ions through the film. A water film placed on top of the ions will retard this ion motion through two effects: (i) Water complexed to the ions increases their size and hence their viscous drag in the 3MP, and (ii) progressively thicker water films will recreate an aqueous phase in which the ions will be fully solvated, generating an energy barrier against ions leaving it.

Films of 3MP were vapor-deposited at 30 K by a molecular beam onto a Pt(111) surface (10 mm in diameter). One monolayer (ML) of 3MP was defined as the amount that saturated its highest temperature peak at about 213 K in temperature-programmed desorption (TPD). Multilayered 3MP desorbs at lower temperatures, starting at 130 K. 3MP is a good glass former—it does not crystallize on Pt(111) up to its desorption temperature (*10*)—and its low-temperature experimental viscosity data are available (*11*).

D_3O^+ ions were produced in an ion source chamber by electron bombardment of D_2O vapor. These ions were extracted and focused by electronic optics, mass-selected by a Wien filter, and decelerated (*12, 13*). The ions were gently landed on the film surface at 30 K at a kinetic energy of 1.0 eV. The ion beam was 9 mm in diameter. A typical ion dose was ~0.15 μC, corresponding to 1.5×10^{12} ions per square centimeter, about 0.1% the surface density of Pt(111).

After ion deposition, various amounts of water were put on top of the ions at 30 K to create an ion-containing water-3MP interface. The water deposition rate was 0.17 "bilayer" per second (1 bilayer = 1.1×10^{15} molecules per square centimeter) (*14*). Finally, the sample was warmed at 0.2 K/s, and voltage changes that reflect the ion motion were measured. A noncontacting McAllister Kelvin probe detected the change in work function ("film voltage") given by $V_f = Qh/\varepsilon_0\varepsilon_s A$, where Q is the total ion charge, h is the mean ion height above the substrate surface (equal to the film thickness if all of the ions were on top of the film), A is the area, ε_0 is the vacuum permittivity, and ε_s is the dielectric constant of the organic film. For hydrocarbon films such as 3MP, their dielectric constants (about 1.9) do not change appreciably with temperature (*15*). Therefore, any large change in V_f corresponds to ion movements in the film. [Not shown here are well-understood (*16*) changes in V_f below 80 K, due to relaxation of slight net alignments of the molecular dipoles of water and 3MP molecules in the films. This alignment occurs during vapor growth from the asymmetry of the vacuum-solid interface.]

Some representative plots of V_f versus temperature T for hydronium ions on a 3MP film of 83 ML (29.5 nm) are shown in Fig. 2. In each curve, there are three temperature regions: (i) Initially, the film voltage hardly changes, indicating that D_3O^+ does not move. (ii) As T increases, V_f abruptly drops to zero in a narrow temperature range of about 10 K at low H_2O coverages, implying that the ions completely move across the 3MP film. (iii) During further temperature ramping, V_f stays near zero. The desorption temperature for 83-ML 3MP peaks at 131 K at low water coverages, but jumps to 152 K at water coverages above about 15 bilayers (below which TPD shows two desorption peaks at 131 and 152 K whose intensities vary with the top water coverage). The amorphous water forms a fairly impermeable cap, leading to abrupt desorption of 3MP at 152 K. This is because cracks in the cap are presumably formed during the crystallization, and the volatile 3MP rapidly desorbs through these cracks; this is the so-called "molecular volcano" desorption (*17*). The ion motion temperatures are always lower than the desorption temperatures.

The most striking feature in Fig. 2 is that the V_f curve moves to high temperatures as the H_2O coverage increases. It is very sensitive to the H_2O coverage, even in the sub-bilayer region. The D_3O^+ motion in 3MP film is apparently hindered by the addition of H_2O on top of the ions.

In Fig. 3 we plot the temperature where V_f drops to 10% of its initial value against H_2O coverage. As the H_2O coverage increases, the fall-off temperatures shift upward and saturate for H_2O coverages above ~15 bilayers. Temperature shifts in Fig. 3 in excess of a few degrees lead to decreases in solvent viscosity of much more than an order of magnitude. This would require a proportionally large increase in ion size (and thus viscous drag) due to hydration to account for the delayed ion motion. However, there is simply not enough water present to make ion-water balls this big. The solvation effect of the water can explain the large temperature shifts, creating an energy trap near the interface.

If the escape of ions from the trap is rate-limiting relative to the ion drift (*18*), we can use the experimental data to estimate the trap depth. Assuming simple Arrhenius kinetics for the departure of ions from the trap, we obtain $dn/dt = -n\nu \exp[-U_{trap}/RT(t)]$, where n is the number of ions in the trap, ν is the preexponential factor, U_{trap} is the trap

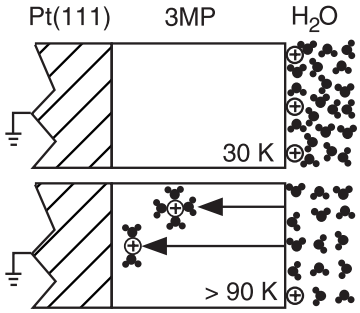

Fig. 1. Schematic drawing of the D_3O^+ ion motion across an H_2O-3MP interface into bulk 3MP. The ions are dosed onto the surface at 30 K, followed by water addition at the same temperature. At 30 K there is insignificant ion motion, as the glassy solvent is too viscous. The ions generate a collective, nearly planar electric field. At higher T (90 K here) the viscosity drops, permitting ions to move into the 3MP, pushed by the field. The ions drag some water molecules with them as they enter the oil phase. Water at coverages greater than a few bilayers creates a solvation energy trap that impedes ion motion into the 3MP.

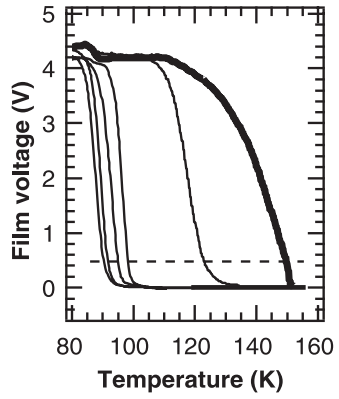

Fig. 2. Film voltage versus temperature as a function of the added water coverage on top of 83-ML 3MP on Pt(111). The film-growth temperature was 30 K, and the temperature ramping rate was 0.2 K per second. The water coverage is (from left to right) 0, 0.50, 1.5, 2.0, 6.0, and 35 bilayers. The dashed line shows the 90% film voltage fall-off temperatures (film voltage has fallen to 10% its original value) to be plotted in Fig. 3.

Pacific Northwest National Laboratory, Box 999, Mail Stop K8-88, Richland, WA 99352, USA.

*To whom correspondence should be addressed. E-mail: jp.cowin@pnl.gov

energy, t is time, and R is the molar gas constant. Because V_f is proportional to n when trapping dominates, the experimental dV_f/dT at 150 K for 35 bilayers of water yields $U_{trap} = 40 \pm 7$ kJ/mol at this water coverage, provided that ν is between 10^{10} and 10^{15} s^{-1}.

We can estimate the water-coverage dependence of the temperature shifts of Fig. 3 with a single fitting parameter, using a modified Born model (*7*) to calculate the solvation energy of the ion. The water and the solvent are represented by continuum films of thicknesses p_w and p_s, and dielectric constants ε_w and ε_s. The ion is at the center of a hollow sphere of radius r_0. The electrostatic energy of the monovalent ion, using a radial field approximation used by Conway (*8*), is a volume integral,

$$U(\vec{r}_{ion}) = \iiint d^3r\left[1 - \frac{1}{\varepsilon(x,y,z)}\right] \times \frac{q_e^2}{32\pi^2\varepsilon_0(\vec{r} - \vec{r}_{ion})^4} \quad (1)$$

where q_e is the electron charge, $\vec{r}_{ion}$ is the position of the ion, and $|\vec{r} - \vec{r}_{ion}| \geq r_0$ (the radius of the hydrated ion). This function readily integrates for slabs of the dielectric, even when the hollow sphere overlaps them. The resultant energies are shown in Fig. 4, along with the slabs for a 20-bilayer water film and the excluded volume of the ion. We used $\varepsilon_w = 200$ and $\varepsilon_s = 1.9$. An unknown parameter is r_0 because we do not know the hydration shell size that might accompany the ion at these temperatures. Using it as a parameter to fit the experimental data gives a value of 4.3 Å (roughly corresponding to the size of the ion with two solvation shells). The case of zero water coverage (curve a) shows that, at $z = 0$, there is a potential that repels the ion away from the vacuum, and a full solvation energy in the 3MP of ~0.7 eV. For the case of 20 bilayers of water (curve g), the ion is strongly attracted toward the water film from both the vacuum and the 3MP. The trap energy is the difference of the potentials at $z = 0$ and deep into the 3MP, and is calculable from Eq. 1 as

$$U_{trap} = \frac{q_e^2}{16\pi\varepsilon_0}\left[\left(\frac{1}{r_0} - \frac{1}{2p_w}\right)\left(1 - \frac{1}{\varepsilon_w}\right) - \left(\frac{1}{r_0} - \frac{1}{2p_s}\right)\left(1 - \frac{1}{\varepsilon_s}\right)\right] \quad p_w \geq r_0$$

$$= \frac{q_e^2}{16\pi\varepsilon_0}\left[\frac{p_w}{2r_0^2}\left(1 - \frac{1}{\varepsilon_w}\right) - \left(\frac{1}{r_0} - \frac{1}{2p_s}\right)\left(1 - \frac{1}{\varepsilon_s}\right)\right] \quad p_w \leq r_0 \quad (2)$$

Referring to Fig. 4, at water coverages below 0.5 bilayer, there is no trap for the ion at the 3MP interface; the ions are repelled by the low-dielectric vacuum. At coverages above 0.5 bilayer, an energy trap near the interface gradually builds up. The trap reaches its maximum above 20 bilayers of water: ~0.40 eV (38 kJ/mol) for the ion motion from the interface into bulk 3MP, and 0.76 eV (73 kJ/mol) from bulk water to bulk 3MP. The latter is very close to the values calculated by molecular dynamics: 71 kJ/mol for the large ion Cs^+ moving from bulk water to bulk carbon tetrachloride (*19*), and 63 kJ/mol for Cl^- transferring from bulk water into 1,2-dichloroethane (*20*).

We can estimate the 90% voltage fall-off temperatures of Fig. 3 using the calculated energy trap from Eq. 2 as a function of water coverage, plus the Arrhenius kinetics for escaping ions with an assumed preexponential of 10^{13} s^{-1}. Because the ion drift kinetics become important at low water coverages, we now include this process for the ions that escape the trap (*18*). The result is shown as the solid curve in Fig. 3. This one-parameter fit ($r_0 = 4.3$ Å) agrees well with the data and demonstrates that the modified Born model, together with the viscosity and kinetics models, predicts very well the hydronium ion motion across the water-3MP interface.

The above calculation could be affected by three complications. First, the ions could have moved to the right of the interface in Fig. 4, into the water layer, as there is a strong potential gradient pushing them in that direction. This effect would precisely double the trap potential and would have required using $r_0 = 8.6$ Å to fit the data, which would correspond to an unphysically large hydration sphere. However, amorphous water is suspected to have a glass transition temperature of 135 K, so the ions should not be able to move into it until above 150 K (*21*).

Second, we have ignored the fact that the collective planar field generated by the ions will lower the trap barrier that the ions encounter. The barrier potential has a slope of 0.044 eV/Å. The collective field varies from zero (for the last ions to leave) to as high as 0.015 eV per ion (for the first ions that leave the trap). The highest field would reduce the barriers shown in Fig. 4 by nearly 50%. To compare with the Born model potential (with no collective fields added), we choose the 90% voltage fall-off temperature at which the initial voltage has fallen to 10% of its original value and the maximum field has been reduced to 0.0015 eV per ion, a negligible value.

We see evidence of the field effects on the barrier in Fig. 2 for the 35-bilayer water curve (thick curve). Some ions escape near 87 K, as the field has decreased the trap barrier to a nearly kinetically insignificant value. The remainder of the ions have a fairly broad range of trap barriers to overcome, as seen from the wide range of temperatures (115 to 150 K) over which they escape. The trap barrier continuously increases as more ions leave it because the collective field is less on the remaining ions.

A third, unresolved issue is that the kinetics of molecular diffusion of both water and solvent molecules could be fast enough, at temperatures where highly trapped ions finally move, to permit field-driven geometry changes of the films themselves. We have ample evidence that the geometry of the films is not grossly different than planar, and that the ions stay initially on top when deposited. This comes from the agreement of the measured capacitances versus predicted values for both 30 K deposited "virgin" films and temperature-ramped 3MP films (*18*). Also, the "volcano" desorption of 3MP caused by capping water films (≥15 ML) implies that the water layer remains continuous in the composite films, at least for $T \leq 152$ K.

Our successful recreation of the ion sol-

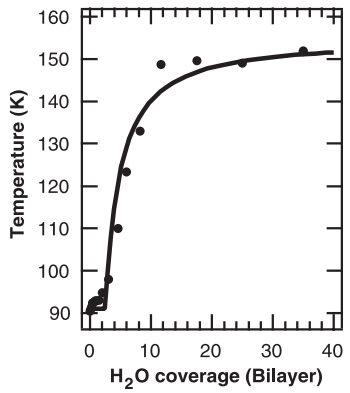

Fig. 3. Experimental 90% film voltage fall-off temperature versus water coverage for 3MP. The combinations of H_2O coverage and temperature that result in the 90% fall-off are shown by solid dots; the solid line is the corresponding theoretical prediction (with one free parameter). The modified Born solvation, viscosity, and kinetics models are used in the calculation. See text for details.

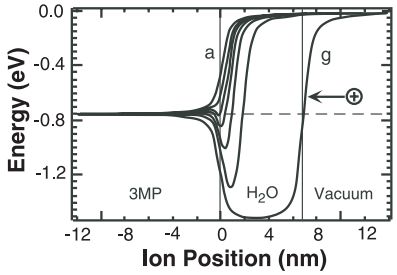

Fig. 4. Theoretically calculated potential change that an ion would undergo during its motion from vacuum through the aqueous phase and bulk 3MP as a function of the water coverage. No collective planar field from the ions is included. The added water coverage for the calculated energy curves (from a to g) is 0, 0.50, 1.0, 1.5, 2.5, 5.0, and 20 bilayers. The zero ion position means the ion is at the water-3MP interface.

vation process, on a molecular layer basis, holds the possibility for many exciting future experiments. An obvious one is to probe how electric fields alter the ion's ability to penetrate the water-oil interfacial barrier. Another possibility takes advantage of the much faster net motion of ions relative to neutrals at these field strengths: We can epitaxially create structured liquids and measure ion motion or trapping in them. In this way we can closely mimic complex interfaces in electrochemistry and in cell membranes.

References and Notes

1. D. A. Doyle *et al.*, *Science* **280**, 69 (1998).
2. R. K. Sen, E. Yeager, W. E. O'Grady, *Annu. Rev. Phys. Chem.* **26**, 287 (1975).
3. C. M. Starks, C. L. Liotta, M. Halpern, *Phase-Transfer Catalysis—Fundamentals, Applications and Industrial Perspectives* (Chapman & Hall, New York, 1994).
4. W. Mitchell Jr., *Fuel Cells* (Academic Press, New York, 1963).
5. R. Noyes, *Nuclear Waste Cleanup Technology and Opportunities* (Noyes, Park Ridge, NJ, 1995).
6. H. E. Allen, *Metal Contaminated Aquatic Sediments* (Ann Arbor Press, Chelsea, MI, 1995).
7. M. Born, *Z. Phys.* **1**, 45 (1920).
8. E. Conway, *J. Electroanal. Chem.* **65**, 491 (1975).
9. I. Benjamin, *Annu. Rev. Phys. Chem.* **48**, 407 (1997).
10. D_3O^+ motion follows the same pattern in 3MP films regardless of the temperature (30 to 125 K) at which they are annealed or grown.
11. A. C. Ling and J. E. Willard, *J. Phys. Chem.* **72**, 1918 (1968).
12. J. P. Cowin, A. A. Tsekouras, M. J. Iedema, K. Wu, G. B. Ellison, *Nature* **398**, 405 (1999).
13. J. P. Biesecker *et al.*, *Rev. Sci. Instrum.* **69**, 485 (1998).
14. A complete, bulk ice–like layer of water has molecules in two slightly separated planes and is traditionally termed a "bilayer" rather than a monolayer. See N. Materer *et al.*, *Surf. Sci.* **381**, 190 (1997).
15. D. R. Lide, *CRC Handbook of Chemistry and Physics* (CRC Press, Boca Raton, FL, 1997), pp. 6–104.
16. M. J. Iedema *et al.*, *J. Phys. Chem. B* **103**, 9203 (1998).
17. R. S. Smith, C. Huang, E. K. L. Wong, B. D. Kay, *Phys. Rev. Lett.* **79**, 909 (1997).
18. A. A. Tsekouras, M. J. Iedema, J. P. Cowin, *J. Chem. Phys.* **111**, 2222 (1999).
19. L. X. Dang, *J. Phys. Chem.* **103**, 8195 (1999).
20. I. Benjamin, *Science* **261**, 1558 (1993).
21. The V_f versus T curve for D_3O^+ on thick amorphous water-ice film (>50 bilayers) grown at 30 K showed that the ions did not move until 150 K, although V_f did drop below 120 K because of the turning-on of the dielectric constant of the amorphous ice. See, for example, A. A. Tsekouras, M. J. Iedema, J. P. Cowin, *Phys. Rev. Lett.* **80**, 5798 (1998).

22. Supported by the U.S. Department of Energy (DOE) Basic Energy Sciences, and performed at the Wiley Environmental Molecular Sciences Laboratory, sponsored by the DOE Office of Biological and Environmental Research. Pacific Northwest National Laboratory is operated by Battelle (contract DE-AC06-76RLO 1830). We thank A. A. Tsekouras for assistance in the early stages of the experiment. K.W. dedicates this paper to Professor Xiexian Guo (1925–1998).

9 September 1999; accepted 9 November 1999

Oligotrophy and Nitrogen Fixation During Eastern Mediterranean Sapropel Events

Julian P. Sachs[1]* and Daniel J. Repeta[2]

Nitrogen isotopic measurements in fossil chlorophyll from late Pleistocene organic-rich sediments (sapropels) in the eastern Mediterranean Sea provide geochemical evidence for stratified, nutrient-depleted surface water and extensive nitrogen fixation. This evidence is reconciled with previous indications of high productivity by invoking a model of sapropel formation in which increased river discharge facilitates development of a specialized phytoplankton population whose annual mass sinking provides the organic flux to generate sapropels. This interpretation is consistent with the widespread occurrence of mat-forming diatoms that thrive in stratified water and can harbor diazotrophic bacterial symbionts, but does not support eutrophication of surface waters by enhanced river runoff or a circulation reversal.

The eastern Mediterranean Sea is a well-ventilated, nutrient-depleted basin (*1*) characterized by low primary productivity (*2*) and organic-deficient sediments (*3*). However, during the late Pleistocene, a series of organic-rich sequences, sapropels, were deposited under what must have been dramatically different depositional conditions than those of today (*4*). These green-brown to black deposits with organic carbon concentrations of 2 to 5% are interspersed between gray nannofossil and foraminiferal marl oozes with organic carbon concentrations of 0.1 to 0.3% (*3*, *5*). They are typically 1 to 30 cm thick (*4*), were formed over periods of 1000 to 10,000 years, and appear to be basin-wide events at water depths below 300 m (*6*). Seven sapropels, numbered S7 through S1, were deposited during the last 200,000 years, the most recent of which occurred in the early Holocene (*4*). The cause of these sedimentary layers is most likely enhanced primary productivity and fluxes of organic carbon to the seafloor (*3*, *7*, *8*), improved preservation rates of organic matter in oxygen-deficient water (*9*), or a combination of the two (*6*, *10*). We conclude from nitrogen isotopic ratios in chlorophyll derivatives (chlorins) that surface waters were oligotrophic, deep waters were anoxic, and nitrogen fixation was widespread during these events. By invoking micropaleontological-based models of sapropel formation (*6*, *7*, *11*) in which increased river runoff induces shoaling of intermediate waters, the formation of a deep algal community, and diminished deep-water ventilation, we reconcile these findings with existing evidence for high export production.

Large fluctuations in sedimentary nitrogen isotopic ratios occur when sapropel layers are present. Whole-sediment $\delta^{15}N$ (*12*) values within sapropels S2 through S7 are nearly constant at $-0.1 \pm 0.5‰$ ($\pm 1\sigma$; $n = 26$) and significantly lower than non-sapropel values between those events (Fig. 1, B and C) that average $5.3 \pm 1.0‰$ ($n = 27$), irrespective of sample age or core location. There are two fundamentally different interpretations of these data. One is that the non-sapropel $\delta^{15}N$ value of 5.3‰ represents the sinking flux of nitrogen, or new production, under normal, oligotrophic conditions, and the sapropel $\delta^{15}N$ value of $-0.1‰$ indicates new production from nutrient-replete surface waters (*5*). As demonstrated in a variety of oceanographic settings, high nutrient concentrations in surface waters lead to the production of organic matter with low $\delta^{15}N$ values (*13*) because faster uptake kinetics cause preferential assimilation of ^{14}N (relative to ^{15}N) when nutrients are abundant (*14*). Our alternative interpretation of the sedimentary $\delta^{15}N$ record is that the low values in sapropels are typical of eastern Mediterranean new production both today and throughout the late Pleistocene, and the high values in organic-deficient marl sediments result from extensive diagenetic alteration of nitrogen isotopic ratios in the presence of oxygen.

Support for our interpretation comes from nitrogen isotopic measurements of contemporary and fossil chlorins and dissolved nitrate. These measurements demonstrate that the contemporary eastern Mediterranean is characterized by very low isotopic values of phytoplankton and deep-water nitrate (Fig. 1A) that are similar to phytoplankton and sedimentary $\delta^{15}N$ values in all six sapropels studied (Fig. 1, B and C). The deposition of recent (non-sapropel) sediments with a $\delta^{15}N$ value of 4.3‰ (Fig. 1A) is an enigma that must be reconciled with the very low isotopic values of reactive nitrogen reservoirs within the eastern Mediterranean.

We determined the nitrogen isotopic composition of living and ancient phytoplankton by measuring the $\delta^{15}N$ value of chlorins (*15*) and correcting for an empirically determined isotopic difference between chlorophyll and total

[1]Department of Environmental Science, Barnard College, Columbia University, 3009 Broadway, New York, NY 10027, USA. [2]Department of Marine Chemistry and Geochemistry, Woods Hole Oceanographic Institution, Woods Hole, MA 02543, USA.

*To whom correspondence should be addressed. E-mail: jpsachs@barnard.columbia.edu